Marine Electrical Sensing for Detecting Small Inhomogeneities

Marine Electrical Sensing for Detecting Small Inhomogeneities

Nick Polydorides, *Member, IEEE,* and Fabrice Delbary.

ABSTRACT

We consider towed electrical sensing for detecting and localising small inhomogeneities in the marine environment. Assuming the domain to be homogeneous apart from a few dispersed inclusions, the low-frequency electrical measurements can be modelled using a single layer potential formulation for a source function defined at the boundaries of the inclusions. A key component of these measurements is the potential induced by the polarisation of the inclusions, which at the far-field can be shown to be equivalent to the potential of dipole sources centred at the inclusions. Under this approximation we formulate an inverse problem for localising the inclusions and then enforce some regularisation in the form of an a priori assumption on the shape of the inclusions. In this context, solving the inverse problem requires tracing some coordinates where the polarisation potential at the current injecting electrodes becomes zero, since these define a set of lines intersecting at the centre of the targeted inclusions. This methodology is implemented by a simple algorithm, whose computational complexity mounts to solving a small number of low-dimensional linear systems. Analysis indicates a fair robustness of

N. Polydorides is with the Institute of Digital Communications, School of Engineering, University of Edinburgh, Edinburgh, EH9 3JL, UK e-mail: N.Polydorides@ed.ac.uk.

F. Delbary is with the Department of Mathematics, University of Genoa, Italy.

the algorithm to measurement noise and model inaccuracies, and this is also supported by numerical simulation experiments.

Index Terms

Towed electrical survey, polarisation induced potential, single layer potential formulation, electric dipole approximation.

I. Introduction

In towed marine electrical sensing, a long elastic cable equipped with a number of electrodes is typically towed near the surface of the sea or at the seabed. While the cable is in motion, low-frequency electric currents are applied through some of the electrodes and the induced electric potentials are sampled on others. This data acquisition cycle iterates at regular time intervals gathering information throughout the domain to be surveyed. As the sea water is conductive to electric current, the sensitivity of these measurements to the electrical conductivity spans a considerable distance, both horizontally and vertically, subject to the magnitude of the applied currents. It is thus unsurprising, that marine electrical sensing has found numerous applications in geophysical investigations, including maritime archaeology [1], environmental surveys [2], forensic investigations [3] and hydrocarbon exploration [4]. In these applications one typically utilises these voltage measurements in order to image the electrical properties of the water column and the sub-seabed sediment. The image reconstruction problem is quite similar to that of electrical resistivity tomography (ERT) [5], a well documented, ill-posed nonlinear inverse problem, but it differs in that the positioning of the electrodes changes dynamically in response to the motion of the towing vessel and the arbitrary sea currents in the vicinity of the cable [6].

Most image reconstruction algorithms for electrical tomography rely on the sensitivity of the voltage measurements to the electrical conductivity of the medium of interest, see for example the relevant chapters in [7] and [8]. These sensitivity-based approaches, are well suited for quantitative conductivity imaging, but despite their popularity, their performance is compromised as the sensitivity drops expo-

nentially away from the electrodes. Consequently, even moderate conductivity variations occurring far from the electrodes have an insignificant impact on the measurements, and are thus rendered electrically unobservable, even in the absence of noise. This is in fact the main reason for the severe ill-posedness of the inverse problem, effectively manifested as a discontinuity in the mapping from the voltage observations to their corresponding conductivity profiles. It is thus reasonable to conclude that sensitivity-based methods are not suitable for imaging or even detecting the small inhomogeneities targeted in this study.

To overcome these limitations some alternative schemes have been proposed, based on layer potential techniques and the use of generalised polarisation and moment tensors, see for example the textbooks [9] and [10] as well as the review [11]. Among them two notable paradigms are the location search methods and the factorisation methods. A location search method for EIT, was proposed in [12], aimed at localising, in real-time, the coordinates of a small, high-contrast, piecewise constant inhomogeneity within the homogeneous unit disk, from a pair of current-voltage observations at its boundary. The authors suggest an easy to implement methodology requiring only the boundary locations of zeros and extrema of the single layer potentials associated with the targeted inclusion. According to [13], the scheme's performance relies strongly on the accurate a priori selection of some free parameters, while any uncertainty in these parameters yields a substantial compromise. The effective dipole method proposed as a location search method in [13], rectifies this shortcoming by postulating that the potential induced by the polarisation of an inclusion can be adequately approximated to the far-field potential of a dipole source, whose moment and magnitude depend on the shape and value of the inhomogeneity. Evidently, this allows one to reformulate the inverse problem of detecting and localising small piecewise constant inhomogeneities to that of localising dipole sources within a homogeneous domain. This problem has been previously studied in the context of electroencephalography and magnetoencephalography [14]. The framework of generalised polarisation tensors is also utilised in [15] and [16] where a simple method for locating a conductivity inclusion and reconstructing its polarisation tensor is developed.

The factorisation methods on the other hand, in contrast to the location search methods, aim not only to localise but also to image the shape of inclusions [17], as long as their conductivities are either higher or lower than that of the hosting medium. These qualitative imaging methods deploy a dense grid of points spanning the domain of interest and then utilise a binary criterion in order to infer whether a point belongs to the closure of an inclusion [18]. The connection between the factorisation method and other methods based on polarisation tensor theory is investigated in [19].

Our approach to localisation is based on the effective dipole formalism [13], while we rely also on [20] for implementing the single layer potential framework. In particular we formulate the inverse localisation problem as a problem of finding the location of an 'equivalent dipole source', by reconstructing its first-order polarisation tensor [11]. As shown in [21] and [22] the shape of an inclusion can be resolved if the high-order polarisation tensors can be reconstructed from the measurements. Moreover the high-order polarisation tensor can distinguish between multiple distinct inclusions positioned close to each other. However, since we have no information on the number of inclusions, their conductivity values or indeed their boundary shape we do not attempt to fit the polarisation potential measurements to the equivalent dipole sources directly, but instead we choose to impose an a priori assumption on the shape of the inclusions and then establish a geometric criterion that yields the locations of the inclusions.

The report is organised as follows: We end this section by introducing some notation, and then proceed to describe the low-frequency electrical measurement in towed motion. In particular we derive the polarisation potential using a single layer potential formulation and show that the charge density involved satisfies a boundary integral equation. Next we address the inverse problem of localising the inhomogeneities, discussing explicitly the dipole approximation of the far-field polarisation potential and the importance of the inclusion's polarisation tensor. The algorithm for solving the inverse problem is presented in the next section, supported by the derivation of a geometric criterion based on the dipole approximation and an a priori assumption on the shape of the inclusions, designed to eradicate the

non-uniqueness of the solution. Finally we present a brief noise analysis of the algorithm and a note on de-noising the measurements, followed by a numerical results section including some simulation tests designed to demonstrate the performance of the algorithm.

A. Notation and symbols

We denote with $\mathcal{C}$ the unbounded two-dimensional domain $\mathbb{R}^2$ where the one-dimensional electric array profile $\mathcal{S}$ is embedded, and specify location by z. In towed motion $\mathcal{S}^t \subset \mathcal{C}$ indicates the support of the array at time t. The domain $\mathcal{C}$ is assumed homogeneous with electrical conductivity σ_h apart from a small unknown number N_Ω of bounded connected Lipschitz inclusions Ω_i whose closures are pairwise disjoint, with uniform conductivities $\sigma_1, \ldots, \sigma_{N_\Omega} \neq \sigma_h$. For an inclusion, $\partial\Omega$ denotes the boundary, $|\Omega|$ the area, ν the outward pointing unit normal vector on $\partial\Omega$, $\overline{\Omega}$ the closure, and $z_{\mathrm{g}} \in \mathcal{C}$ the coordinates of its geometric centre. Two important coordinates on the towed cable are $z_{\mathrm{p}} \in \mathcal{S}^t$ and $z_{\mathrm{m}} \in \mathcal{S}^t$, denoting the positively and negatively charged electrodes respectively, through which the current is applied. The electric potential generated in these conditions will be expressed as $u(z,t)$, emphasising its dependance on location and time where appropriate or simply $u(z)$ when we refer to the potentials at arbitrary times. With u_+ (u_-) we express the trace of u on $\partial\Omega$ from the outside (respectively inside), $\partial_\nu u$ denotes the normal component of the gradient of the potential at $\partial\Omega$, $\partial_\nu u_+$ ($\partial_\nu u_-$) is the normal derivative of the electric potential from the outside (respectively inside) of $\partial\Omega$, and $\partial_z u$ is the gradient of the potential along $\mathcal{S}$. The physical medium to which $\mathcal{S}$ corresponds is a flexible cable, also known as electric array, of length l and diameter d, towed neutrally buoyant at a constant speed τ along a survey trajectory that is independent to the location of the inclusions. In the model of the cable's motion $T(z)$ denotes the tension profile on $\mathcal{S}$, as a result of the towing force and the hydrodynamic loads, ρ is the density of sea water, κ_t and κ_n are the cable's tangential and normal drag coefficients, and $\theta(z)$ is the cable's orientation angle. The tangential and normal velocity profiles of the cable are expressed by $a_t(z)$ and $a_n(z)$, while $c_t(z)$ and $c_n(z)$ denote the corresponding components

of the sea currents. The schematic diagram in figure 1 illustrates the system in consideration.

Considering an open subset V of $\mathbb{R}^2$, $L^2(V)$ and $L^2(\partial V)$ denote respectively the Hilbert spaces of Lebesgue square-integrable functions on V and ∂V. $H^1(V)$ denotes the Hilbert space of functions in $L^2(V)$ whose first derivative in the sense of distributions is in $L^2(C)$. $H^1_{\mathrm{loc}}(V)$ denotes the topological space of functions f on V such that $f|_K \in H^1(\mathring{K})$ for all compact subsets K of V. Consider now that V is a Lipschitz domain, then $H^{1/2}(\partial V)$ denotes the Hilbert space of functions φ in $L^2(\partial V)$ such that the function $(x,y) \mapsto \dfrac{|\varphi(x)-\varphi(y)|}{|x-y|}$ is in $L^2(\partial V \times \partial V)$. $H^{-1/2}(\partial V)$ denotes the dual space of $H^{1/2}(\partial V)$. Denoting by $V_i, i = 1, \dots N_V$ the connected components of V ($N_V = 1$ if V is connected), $H^{-1/2}_{\diamond}(\partial V)$ denotes the space of functions φ in $H^{-1/2}(\partial V)$ such that $\displaystyle\int_{\partial\Omega_i} \varphi \,\mathrm{d}s = 0\,,\ i = 1 \dots N_V$, where by abuse of notation, for $i = 1 \dots N_V$, $\displaystyle\int_{\partial\Omega_i} \varphi \, ds$ denotes the duality product of φ and the constant function of value 1, which is in $H^{1/2}(\partial V_i)$.

II. The electromechanical model

We begin by approximating the three-dimensional system on the horizontal plane by considering the domain's *depth-averaged bulk conductivity*

$$\sigma(z) = \frac{1}{d_\sigma} \int_{\mathcal{C}_z} \sigma_{3\mathrm{d}}(z, z_\perp) \,\mathrm{d}z_\perp, \quad z \in \mathcal{C}, \tag{1}$$

as a volume integral of the conductivity function $\sigma_{3\mathrm{d}}$ over a cylindrical domain $\mathcal{C}_z$ of infinitesimal radius, centred at z, aligned orthogonally to the plane $z_\perp = 0$ and extending to a depth d_σ according to the electric field penetration. In this context let the piecewise constant conductivity within the domain of interest to be defined by

$$\sigma(z) = \begin{cases} \sigma_h & z \in \mathcal{C} \setminus \displaystyle\bigcup_{i=1}^{N_\Omega} \overline{\Omega}_i \\ \sigma_i & z \in \Omega_i \end{cases} \tag{2}$$

where N_Ω is the unknown number of inclusions, where $\sigma_i \neq \sigma_h$. Applying a current pattern of the form

$$f = i_f \big[\delta(z - z_{\mathrm{p}}) - \delta(z - z_{\mathrm{m}})\big], \ \ z_{\mathrm{p}}, z_{\mathrm{m}} \in \mathcal{S}^t, \tag{3}$$

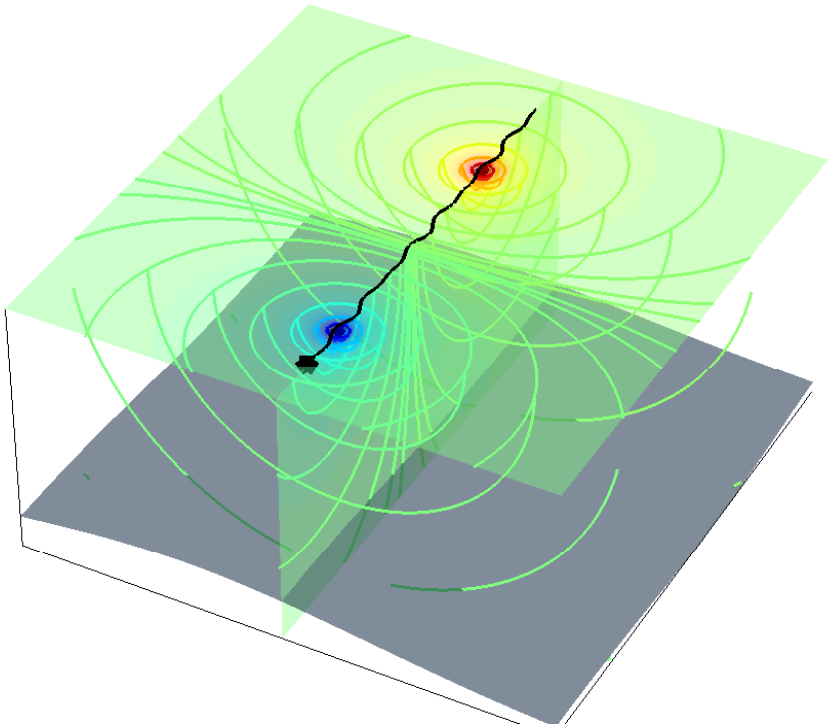

Fig. 1. A schematic diagram for the marine electrical sensing application. A slender electric array (black line) is towed neutrally buoyant while it acquires electrical data. The figure shoes the electric potential field at two perpendicular planes intersecting near the support of the array: the horizontal plane considered in this study, and the vertical one utilised in marine resistance tomography applications. The field symmetry allows one to consider either of the these planes in approximating the problem in two-dimensions. The potential field in this illustration is based on the free space Green's function for the three-dimensional Laplacian equation.

where δ is the Dirac function and i_f the magnitude of the current yields an electric potential $u \in H^1_{\rm loc}(\mathcal{C} \setminus \{z_{\rm p}, z_{\rm m}\})$ that verifies the generalised Poisson equation

$$-\nabla \cdot \sigma(z) \nabla u(z) = f(z, z') \ \text{ in } \ \mathcal{C}, \ z' \in \mathcal{S}^t. \tag{4}$$

Since the domain is unbounded the electric potential satisfies the decay condition

$$u(z) \underset{|z| \to \infty}{=} O(|z|^{-1}), \tag{5}$$

uniformly in all directions, thus the potential field we seek to measure belongs in the subspace of $H^1_{\rm loc}(\mathcal{C} \setminus \{z_{\rm p}, z_{\rm m}\})$ that conforms the decay condition (5). The location of the current source function as well as the coordinates of the electrodes that measure u depend on the position and shape of the cable at any given time. Assuming the velocity of the towing vessel is kept almost constant in magnitude the motion of the cable can be approximated by the linear hydrodynamic model [23]

$$\partial_z T(z) = \frac{1}{2}\rho\pi d\kappa_t\big(a_t(z) - c_t(z)\big)\big|a_t(z) - c_t(z)\big|, \tag{6}$$

$$T(z)\,\partial_z\theta(z) = \frac{1}{2}\rho d\kappa_n\big(a_n(z) - c_n(z)\big)\big|a_n(z) - c_n(z)\big|, \tag{7}$$

$$\partial_t\theta(z) = \partial_z a_n(z) + a_t(z)\partial_z\theta(z), \tag{8}$$

$$\partial_z a_t(z) = a_n(z)\partial_z\theta(z), \tag{9}$$

for $z \in \mathcal{S}^t$ yielding the velocity, tension and position of the cable subject to the influence of the towing velocity and the impinging ocean currents. The array is hinged to the towing vessel, hence the velocity components at its head satisfy

$$a_t(z_0) = \tau_x(t)\cos\theta(z_0) + \tau_y(t)\sin\theta(z_0), \tag{10}$$

$$a_n(z_0) = -\tau_x(t)\sin\theta(z_0) + \tau_y(t)\cos\theta(z_0), \tag{11}$$

where $z_0 \in \mathcal{S}^t$, $\tau_x(t)$ and $\tau_y(t)$ are the Cartesian components of the vessel's velocity at time t. At the other end a buoy is attached in order to keep the tail of the cable straight, effectively causing

$$T(z_{\rm l}) = |\tau|^{-2}T_l\sqrt{\big(a_t^2(z_{\rm l}) + a_n^2(z_{\rm l})\big)}, \tag{12}$$

for some known $T_l > 0$ tension value, while the zero tail curvature constraint essentially translates to

$$a_n(z_{\rm l}) = c_n(z_{\rm l}), \quad \text{for all } t. \tag{13}$$

Under the conditions (6)-(13) the motion of the cable is uniquely determined to yield the coordinates of the applied currents and measured voltages, within the numerical error margin [23]. In addition to the electrical measurements, data acquisition involves also positioning measurements of the electrodes in short, regular time intervals.

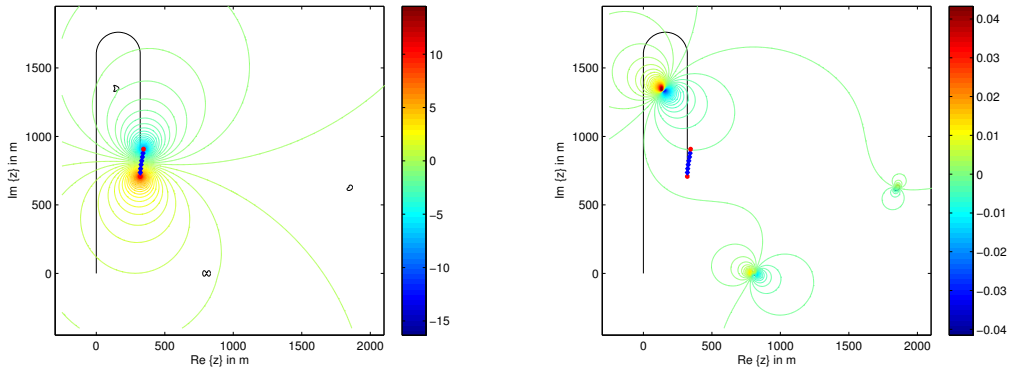

Fig. 2. Left the electric potential field at a certain time instant of the survey, and right the polarisation induced potential field due to three inclusions: $\sigma_1 = 10^{-3}$ S/m (kite, left), $\sigma_2 = 10^{-1}$ S/m (peanut, middle) and $\sigma_3 = 10^{2}$ S/m (bean, right), immersed in a background of 1 S/m. The solid line marks the towing vessel trajectory, the red markers are the current applying electrodes and the blue the positions of the other electrodes on the 500 m long array. Note the difference in the magnitude of the two potential fields.

The ocean currents, although arbitrary and time-varying, are assumed known in simulating the motion of the cable. Knowing their profile is not a requirement for localising the inclusions, although these can be estimated using the methodology described in [23]. Their scope in this study is predominantly to make the towing motion of the cable as realistic as possible, so that the trajectory of the cable differs from that of the towing vessel. Effectively, this introduces the additional complexity of not knowing a priori the exact location of the electrodes.

The position of the cable, and hence that of the electrodes, is measured using accelerometers embedded in the cable. For electric arrays, the commercial standard involves fibre-optics based accelerometers, that are accurate to about a centimetre. In conjunction with the global positioning system that is typically mounted on the towing vessel, the positioning network resolves the coordinates of the cable every one or two seconds. Tracking the position and curvature of the cable with accuracy is important, therefore the analysis section addresses the performance of the proposed localisation algorithm against the inevitable positioning errors and uncertainties.

III. THE DIRECT PROBLEM

We consider the problem of computing the electric potential field u in the conductive domain $\mathcal{C}$ when a low-frequency current f is applied through the electrodes of the cable $\mathcal{S}^t$. For notational clarity we derive the formulation of the potential assuming one inclusion.

The polarisation potential admits a single layer formulation and the total potential field satisfies

$$u(z) = u^h(z) + \sum_{i=1}^{N_\Omega} v_i(z), \quad z \in \mathcal{C}. \tag{14}$$

Since σ_h and σ (where σ would be equivalent to σ_i for a multiple inclusion configuration) are constant, u is the solution of (4) iff u is harmonic in Ω and $\mathcal{C} \setminus (\overline{\Omega} \cup \{z_{\rm p}, z_{\rm m}\})$ and also verifies the continuity conditions at the interface of the inclusion

$$\begin{aligned} u_+(z) &= u_-(z), \quad z \text{ on } \partial\Omega \\ \sigma_h \partial_\nu u_+(z) &= \sigma \partial_\nu u_-(z), \quad z \text{ on } \partial\Omega \end{aligned} . \tag{15}$$

Considering $u^h \in H^1_{\rm loc}(\mathcal{C} \setminus \{z_{\rm p}, z_{\rm m}\})$ defined by

$$u^h(z) = \frac{i_f}{\sigma_h}\big[\Phi(z - z_{\rm p}) - \Phi(z - z_{\rm m})\big], \tag{16}$$

where Φ is the fundamental solution of the Laplace equation

$$\Phi(z - z') = \frac{1}{2\pi} \ln \frac{1}{|z - z'|}\ , \ z \neq z', \tag{17}$$

u^h is the homogenous electric potential in $\mathcal{C}$ such that

$$-\nabla \cdot \sigma_h(z) \nabla u^h(z,t) = f, \ \ z \in \mathcal{C} \setminus \{z_{\rm p}, z_{\rm m}\}, \tag{18}$$

and u^h verifies the decay condition (5). When a bounded inhomogeneity Ω appears in the support of the electric potential u^h, then that inclusion is said to be polarised by this potential. In turn, this induces a surface charge density at its boundary yielding a polarisation potential v [11]. In these conditions, the total potential field can be decomposed in the homogeneous and inhomogeneity-induced polarisation potentials

$$u(z) = u^h(z) + v(z), \quad z \in \mathcal{C} \setminus \{z_{\rm p}, z_{\rm m}\}, \tag{19}$$

where u is the solution of (4) and (5) iff $-\Delta v(z) = 0$ in Ω and $\mathcal{C} \setminus \overline{\Omega}$ and verifies the continuity conditions

$$\begin{aligned} v_+(z) &= v_-(z), \quad z \text{ on } \partial\Omega \\ v_+(z) \times \nu &= v_-(z) \times \nu, \quad z \text{ on } \partial\Omega \\ \sigma_h \partial_\nu v_+(z) - \sigma \partial_\nu v_-(z) &= -(\sigma_h - \sigma)\partial_\nu u^h(z), \quad z \text{ on } \partial\Omega \end{aligned} \tag{20}$$

as well as the decay condition (5) away from the inclusion. For a bounded inclusion Ω with Lipschitz continuous boundary $\partial\Omega$, given an integrable current density function $\varphi \in H^{-1/2}(\partial\Omega)$, the polarisation potential can be expressed as a single layer potential [9]

$$v(z) = \int_{\partial\Omega} \Phi(z - z')\varphi(z') \, \mathrm{d}s(z'), \quad z \in \mathcal{C} \setminus \partial\Omega, \; z' \in \partial\Omega, \tag{21}$$

so that v is harmonic in Ω and $\mathcal{C} \setminus \overline{\Omega}$ and continuous across the interface $\partial\Omega$. By virtue of the jump condition of the normal derivative of the single layer potential

$$\partial_\nu v_\pm(z) = \mp \frac{\varphi(z)}{2} + \int_{\partial\Omega} \partial_{\nu(z)} \Phi(z - z')\varphi(z') \, \mathrm{d}s(z'), \quad z \in \partial\Omega, \tag{22}$$

v verifies the last continuity condition of (20) iff φ is solution of the boundary integral equation of the second kind [20]

$$\varphi(z) - \mu \mathbf{K}'\varphi(z) = 2\mu \partial_\nu u^h(z), \tag{23}$$

for a conductivity contrast coefficient

$$\mu = \frac{\sigma_h - \sigma}{\sigma_h + \sigma}, \tag{24}$$

and $\mathbf{K}' : H^{-1/2}(\partial\Omega) \to H^{-1/2}(\partial\Omega)$ a bounded operator defined by

$$(\mathbf{K}'\varphi)(z) = 2 \int_{\partial\Omega} \partial_{\nu(z)} \Phi(z - z') \; \varphi(z') \, \mathrm{d}s(z'), \quad z \in \partial\Omega, \tag{25}$$

and

$$\int_{\partial\Omega} \varphi(z') \mathrm{d}s(z') = 0. \tag{26}$$

The integrals in (25) and (22) are to be considered in their Cauchy principal value sense, while (26) ensures the potential decay condition $v(z) = O(|z|^{-1})$ away from the inclusion. The normal component

of the gradient of the potential across $\partial\Omega$ verifies the jump conditions

$$\varphi(z) = \partial_\nu v_-(z) - \partial_\nu v_+(z) \;\; z \text{ on } \partial\Omega \tag{27}$$

$$= \partial_\nu u_-(z) - \partial_\nu u_+(z) \;\; z \text{ on } \partial\Omega. \tag{28}$$

The equality (27) follows from

$$\partial_\nu v_\pm(z) = \frac{1}{2}\big(\mp\mathbf{I} + \mathbf{K}'\big)\varphi(z), \;\; z \in \partial\Omega,$$

(c.f. (25) - (22)) by solving for $\partial_\nu u_-(z) - \partial_\nu u_+(z)$, and the one in (28) is due to the potential decomposition $u^h = u_+ - v_+ = u_- - v_-$ from where we obtain $u_+ - u_- = v_+ - v_-$. Notice that although u and u^h are singular at the charged electrodes, v tends to be smooth throughout $\mathcal{S}^t$ when the inclusion is away from the cable. Figure 2 depicts the two components of the potential field for an arbitrary cable profile $\mathcal{S}^t$, indicating also the scale difference in their respective magnitudes. In the case for multiple inclusions, as treated in (Theorem 2.9) of [11], the surface current densities φ_i, $i = 1, \ldots, N_\Omega$ are defined uniquely and satisfy

$$\sum_{j=1}^{N_\Omega} (\mathbf{I} - \mu_i \mathbf{K}'_{ij})\varphi_j(z) = 2\mu_i \partial_\nu u^h(z), \quad z \in \partial\Omega_i, \tag{29}$$

where $\mathbf{K}'_{ij} : H_\diamond^{-1/2}(\partial\Omega_j) \to H_\diamond^{-1/2}(\partial\Omega_i)$ is defined by

$$(\mathbf{K}'_{ij}\varphi)(z) = 2\int_{\partial\Omega_j} \partial_{\nu(z)}\Phi(z - z')\, \varphi(z')\, \mathrm{d}s(z'), \quad z \in \partial\Omega_i. \tag{30}$$

This yields a potential field

$$u(z) = u^h(z) + \sum_{i=1}^{N_\Omega} \int_{\partial\Omega_i} \Phi(z - z')\varphi_i(z')\, \mathrm{d}s(z'), \quad z \in \mathcal{C} \setminus \partial\Omega_i, \; z' \in \partial\Omega_i. \tag{31}$$

Note that according to (Theorem 2.9) of [11]

$$\varphi_i(z) = 2\mu_i(\mathbf{I} - \mu_i \mathbf{K}'_{ii})^{-1}\partial_\nu u^h(z) + O(\Delta z^{-2}), \tag{32}$$

where $\Delta z = \min\{|z_{\mathrm{g}i} - z_{\mathrm{g}j}| : i \neq j\}$. This derivation relies on the assumption that none of the active electrodes resides within the inclusion [24]. From a practical prospective this is indeed a realistic

scenario considering that the targeted inhomogeneities are few in number, highly dispersed, and of very small diameters by comparison to the length of the cable. The case of a cluster is treated in [24] where it is shown that the cluster's polarisation tensor can be approximated to that of an inclusion of elliptic shape. Although unlikely, if any of the electrodes enters the closure of the inclusion then this will likely be manifested by the abrupt change in the electrical measurements. For the sake of completeness in our derivation, note that if both active electrodes enter Ω, then the imposed potential trivially changes to

$$u^h(z) = \frac{i_f}{\sigma}\big[\Phi(z - z_{\rm p}) - \Phi(z - z_{\rm m})\big] \tag{33}$$

while everything else remains the same, however if one of the two electrodes, for example $z_{\rm p}$, enters Ω, then

$$u^h(z) = i_f\big[\frac{1}{\sigma}\Phi(z - z_{\rm p}) - \frac{1}{\sigma_h}\Phi(z - z_{\rm m})\big], \tag{34}$$

and now, u^h and v do not verify the decay condition separately, however their sum u does. Similarly, the solution φ to the boundary integral equation now verifies

$$\int_{\partial\Omega} \varphi(z)\, {\rm d}z = \frac{1}{\sigma_h} - \frac{1}{\sigma}. \tag{35}$$

For details on the numerical implementation of the electrical module, including the solution of the boundary integral equation using the Nyström method we refer the reader to [20]. The mechanical module was addressed using a linear finite difference time domain scheme as detailed in [23] and the references therein.

Remark III.1. *The forward problem study has been presented for general Lipschitz inclusions. In the case of more regular inclusions, like C^2, the density function for the single layer potential is in the Hölder space $C^{0,\alpha}(\partial\Omega)$ and the potential is in $C^{1,\alpha}(\mathbb{R}^2 \setminus \Omega)$ and $C^{1,\alpha}(\overline{\Omega})$ [25].*

IV. THE INVERSE PROBLEM

We now address the inverse problem of detecting and localising the inclusions using electrical potential measurements captured on $\mathcal{S}^t$ at discrete regular time instants $t \in \{t_1, t_2, \ldots, t_{\text{end}}\}$. We begin by examining the far-field measurement of the polarisation potential $v(z)$, i.e. through the actual measurements of $u(z)$, in order to assess what information about an inclusion Ω is incorporated in these measurements. Following [11], assume for notational consistency that $z = (z_1, z_2)$ where $z_1 = \Re\{z\}$, $z_2 = \Im\{z\}$ are the cartesian coordinates, and $i, j \in \mathbb{N}^2$ are double-index variables. As per the standard multi-index notation $i! = i_1! i_2!$, $|i| = i_1 + i_2$, $\partial^i f = \partial_1^{i_1} \partial_2^{i_2} f$ and $z^i = z_1^{i_1} z_2^{i_2}$. Since u^h is a harmonic function in $\mathcal{C}$ then it admits a Taylor expansion $u^h(z) = \sum_{|i|=0}^{+\infty} \frac{1}{i!} \partial^i u^h(z_{\text{g}}) z^i$, while the fundamental solution Φ on which u^h depends can now be expressed as $\Phi(z - z') = \sum_{|j|=0}^{+\infty} \frac{(-1)^{|j|}}{j!} \partial^j \Phi(z) z'^j$ as $|z| \to \infty$. Based on these the far-field polarisation potential takes the form of

$$v(z) = \sum_{|i|=1}^{+\infty} \sum_{|j|=1}^{+\infty} \frac{(-1)^{|j|}}{i!j!} \partial^i \Phi(z - z_{\text{g}}) \mathbf{M}_{ij}(\Omega) \partial^i u^h(z_{\text{g}}), \text{ as } |z| \to \infty, \tag{36}$$

where

$$\mathbf{M}_{ij}(\Omega) = \int_{\partial\Omega} z'^j \phi_i(z') \mathrm{d}s(z'), \tag{37}$$

is the generalised polarisation tensor associated with the inclusion Ω and

$$\phi_i(z') = 2\mu(\mathbf{I} - \mu \mathbf{K}')^{-1}(\nu_z \cdot \nabla z^i)(z'), \quad z' \in \partial\Omega. \tag{38}$$

Evidently, at the far-field an inclusion's geometry and conductivity value are observable through its generalised polarisation tensors $\mathbf{M}$, which in the special case where $|i| = |j| = 1$ is a 2×2 symmetric matrix depending on the shape of $\partial\Omega$ and the contrast σ_h/σ (Pólya-Szegö polarisation tensor). Otherwise it is a symmetric tensor in the sense of the theorem 3.8(ii) of [11]. When Ω is a

disk (hence $\partial\Omega$ is a circle on $\mathcal{C}$) with a non-zero radius r and conductivity σ,

$$\begin{aligned}(\mathbf{K}'\varphi)(z) &= 2\int_{\partial\Omega}\partial_{\nu(z)}\Phi(z-z')\varphi(z')\,\mathrm{d}s(z')\\ &= -\frac{1}{\pi}\int_{\partial\Omega}\frac{\langle z-z',\nu(z)\rangle}{|z-z'|^2}\varphi(z')\,\mathrm{d}s(z')\\ &= -\frac{1}{\pi r}\int_{\partial\Omega}\varphi(z')\,\mathrm{d}s(z')\\ &= 0,\end{aligned}$$

hence the jump condition at the boundary of the inclusion reduces to

$$\partial_\nu v_\pm(z') = \mp\frac{\varphi(z')}{2}, \quad z'\in\partial\Omega,$$

while the Pólya-Szegö polarisation tensor admits an explicit expression [9]

$$\mathbf{M}^o(\Omega) = (\sigma_h-\sigma)|\Omega|\begin{pmatrix}\frac{2r}{r(\sigma_h+\sigma)} & 0\\ 0 & \frac{2r}{r(\sigma_h+\sigma)}\end{pmatrix} = 2\mu\pi r^2\mathbf{I}, \tag{39}$$

where $|\Omega|$ is the area of the inclusion. At the far-field $v(z)$ can be approximated to the far-field of an electric dipole source with moment $\mathbf{p}$ centred at z_g. Let the dipole potential be $D_{\mathrm{p}(z_\mathrm{g})}(z)$ then the appropriate dipole moment $\mathbf{p}$ should yield

$$v(z)\approx D_{\mathrm{p}(z_\mathrm{g})}(z) \quad \text{as} \quad |z-z_\mathrm{g}|\to\infty. \tag{40}$$

According to [13], this approximation is accurate to second-order when

$$\mathbf{p} = \mathbf{M}\nabla u^h(z_\mathrm{g}).$$

In the case of multiple inclusions, we have

$$v(z)\approx\sum_{k=0}^{N_\Omega} D_{\mathrm{p}_k(z_{\mathrm{g}_k})}(z) \quad \text{as} \quad |z_{\mathrm{g}_i}-z_{\mathrm{g}_j}|\to\infty \quad \text{for} \quad i\neq j, \tag{41}$$

where

$$\mathbf{p}_k = \mathbf{M}_k\nabla u^h(z_{\mathrm{g}_k}).$$

Note that the above condition depends on the properties of the targeted inclusion(s) through the generalised polarised tensor, hence it is impractical to compute the optimum dipole moment ahead

of reconstructing the inclusion. Invariably, $\mathbf{p}$ does not have a unique representation unless the shape and the conductivity value of the inclusion are specified. To alleviate this difficulty we apply a shape regularity assumption, namely that 'any inclusion will have the shape of a disk'. In effect, we are now considering dipole moments of the form

$$\mathbf{p}^o = \mathbf{M}^o \nabla u^h(z_{\rm g}), \tag{42}$$

such that as $|z - z_{\rm g}| \to \infty$,

$$\begin{aligned} v_o(z) \approx D_{{\rm p}^o(z_{\rm g})}(z) &= \Big\langle \frac{\mathbf{p}^o}{2\pi}, \frac{z - z_{\rm g}}{|z - z_{\rm g}|^2} \Big\rangle \\ &= \mu r^2 \Big\langle \nabla u^h(z_{\rm g}), \frac{z - z_{\rm g}}{|z - z_{\rm g}|^2} \Big\rangle \\ &= -\mu r^2 \frac{i_f}{2\pi\sigma_h} \Big\langle \frac{z_{\rm g} - z_{\rm p}}{|z_{\rm g} - z_{\rm p}|^2} - \frac{z_{\rm g} - z_{\rm m}}{|z_{\rm g} - z_{\rm m}|^2}, \frac{z - z_{\rm g}}{|z - z_{\rm g}|^2} \Big\rangle \end{aligned} \tag{43}$$

where $v_o(z)$ is the far-field polarisation potential expansion (36) with $\mathbf{M} = \mathbf{M}^o$.

V. The algorithm

The algorithm for locating the inclusions is based on the dipole approximation of the polarisation potential for disk shaped inclusions. In particular, it uses two particular measurements in order to locate the geometric centre $z_{\rm g}$ of an inclusion. Each of these 'measurements' corresponds to the coordinates of the active electrodes $z_{\rm p}$ or $z_{\rm m}$ at a certain $\mathcal{S}^t$ where the polarisation induced potential measured there becomes zero. In particular, if there exist $z_{\rm p}^*$ or $z_{\rm m}^*$ such that $v(z_{\rm p}^*) = 0$ or $v(z_{\rm m}^*) = 0$, then the corresponding pairs $(z_{\rm p}^*, z_{\rm m}) \in \mathcal{S}^t$ (or $(z_{\rm p}, z_{\rm m}^*) \in \mathcal{S}^t$) will be utilised for localising the inclusion to which v corresponds. Identifying a pair of such points, by following a simple measurement procedure, yields the definition of two lines embedded in $\mathcal{C}$ that intersect at $z_{\rm g}$. Note that in these measurements, the actual quantity being measured is the total electric potential u, thus what we refer to as measurements here are simply the difference between the measured signal and the homogenous potential field.

To explain how the algorithm works consider that at $z = z_{\rm p}$, the dipole approximation of the

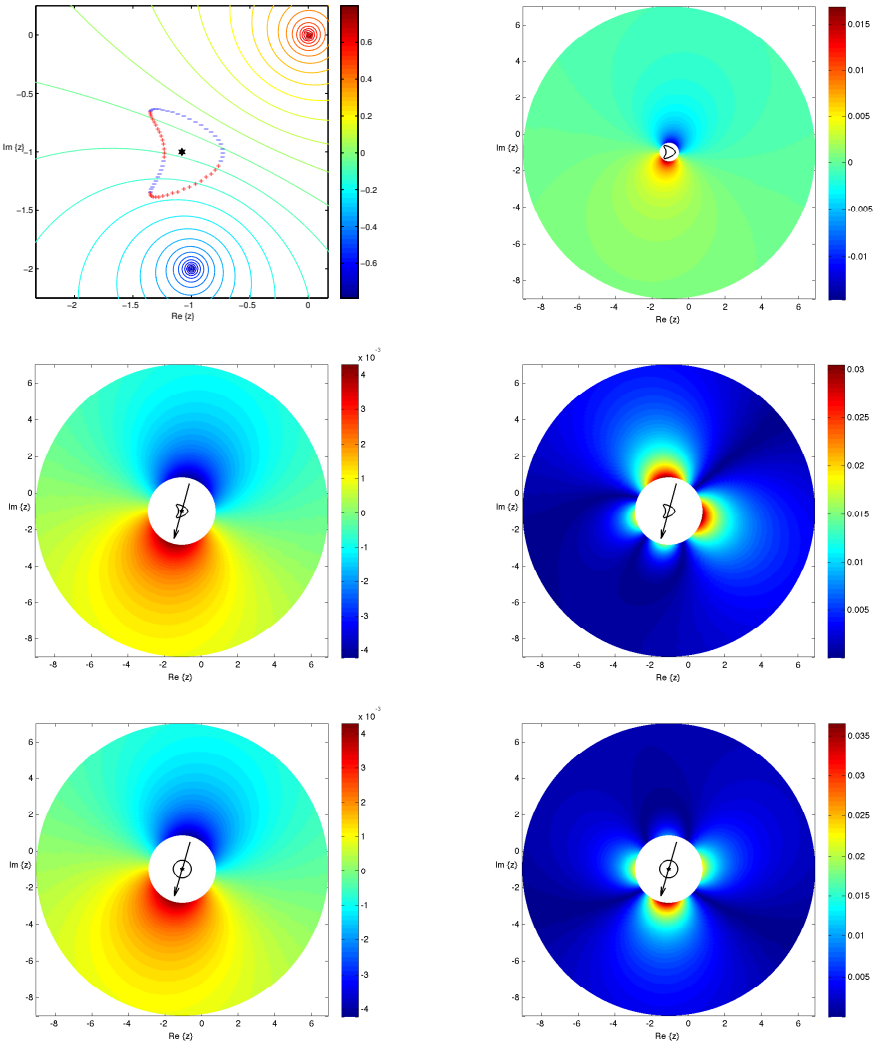

Fig. 3. At the top row, the polarisation of a kite-shaped inhomogeneity by a potential field imposed by a current applied through two point electrodes at $z_{\rm p} = 0$ and $z_{\rm m} = -1-2{\rm i}$. Notice the polarity of the source density function φ defined at the boundaries of the inclusion. At the middle row, the dipole induced potential approximation of the polarisation potential assuming a dipole source whose moment conforms the polarisation tensor of the kite-shaped inclusion. To its right, the relative error in this dipole approximation of the far-field polarisation induced potential. At the bottom row, the dipole potential approximation of the induced potential, this time assuming a dipole moment that conforms a dish-shaped inclusion instead, and next the relative error in the approximation. The figures illustrate the validity of the dipole approximation and the adopted shape regularity assumption.

polarisation potential assuming a disk-shaped inclusion (43) becomes

$$\begin{aligned} D_{\mathrm{p}^o(z_\mathrm{g})}(z_\mathrm{p}) &= \Big\langle \frac{\mathbf{p}^o}{2\pi}, \frac{z_\mathrm{p}-z_\mathrm{g}}{|z_\mathrm{p}-z_\mathrm{g}|^2} \Big\rangle, \\ &= \mu r^2 \frac{i_f}{2\pi\sigma_h} \Big\langle \frac{z_\mathrm{g}-z_\mathrm{p}}{|z_\mathrm{g}-z_\mathrm{p}|^2} - \frac{z_\mathrm{g}-z_\mathrm{m}}{|z_\mathrm{g}-z_\mathrm{m}|^2}, \frac{z_\mathrm{g}-z_\mathrm{p}}{|z_\mathrm{g}-z_\mathrm{p}|^2} \Big\rangle, \\ &\propto \Big\langle \frac{\bar{z}_\mathrm{gp}}{|z_\mathrm{gp}|}, \frac{\bar{z}_\mathrm{gp}}{|z_\mathrm{gp}|} - \frac{\bar{z}_\mathrm{gm}}{|z_\mathrm{gm}|} \Big\rangle, \\ &\propto \Big\langle \bar{z}_\mathrm{gp}, \bar{z}_\mathrm{gp} - \frac{|z_\mathrm{gp}|}{|z_\mathrm{gm}|}\bar{z}_\mathrm{gm} \Big\rangle \end{aligned} \tag{44}$$

where $z_\mathrm{gp} = z_\mathrm{g} - z_\mathrm{p}$, $z_\mathrm{gm} = z_\mathrm{g} - z_\mathrm{m}$ are the displacement vectors, and $\bar{z}_\mathrm{gp} = z_\mathrm{gp}/|z_\mathrm{gp}|$ and $\bar{z}_\mathrm{gm} = z_\mathrm{gm}/|z_\mathrm{gm}|$ their respective unit vectors for $z_\mathrm{p}, z_\mathrm{m} \in \mathcal{S}^t$. Similarly, it can be shown that at $z = z_\mathrm{m}$

$$\begin{aligned} D_{\mathrm{p}^o(z_\mathrm{g})}(z_\mathrm{m}) &= \Big\langle \frac{\mathbf{p}^o}{2\pi}, \frac{z_\mathrm{m}-z_\mathrm{g}}{|z_\mathrm{m}-z_\mathrm{g}|^2} \Big\rangle, \\ &\propto \Big\langle \bar{z}_\mathrm{gm}, \frac{|z_\mathrm{gm}|}{|z_\mathrm{gp}|}\bar{z}_\mathrm{gp} - \bar{z}_\mathrm{gm} \Big\rangle. \end{aligned} \tag{45}$$

Now suppose away from the inclusion there is a point z_p^* where $v(z_\mathrm{p}^*) = 0$. Then subject to the dipole approximation $D_{\mathrm{p}^o(z_\mathrm{g})}(z) \approx v_o(z)$, and the incorporated shape regularity assumption, one may establish the geometric criterion

$$v(z_\mathrm{p}^*) = 0 \quad \Longrightarrow \quad \Big\langle \bar{z}_\mathrm{gp}^*, \bar{z}_\mathrm{gp}^* - \frac{|z_\mathrm{gp}^*|}{|z_\mathrm{gm}|}\bar{z}_\mathrm{gm} \Big\rangle = 0, \tag{46}$$

and respectively for a point z_m^* away from the inclusion,

$$v(z_\mathrm{m}^*) = 0 \quad \Longrightarrow \quad \Big\langle \bar{z}_\mathrm{gm}^*, \frac{|z_\mathrm{gm}^*|}{|\bar{z}_\mathrm{gp}|}\bar{z}_\mathrm{gp} - \bar{z}_\mathrm{gm}^* \Big\rangle = 0. \tag{47}$$

Developing further the criteria (46) and (47) yields a linear system

$$\begin{cases} \langle z_\mathrm{g} - z_\mathrm{m}, z_\mathrm{m} - z_\mathrm{p}^* \rangle &= 0, \\ \langle z_\mathrm{g} - z_\mathrm{p},\, z_\mathrm{p} - z_\mathrm{m}^* \rangle &= 0, \end{cases} \tag{48}$$

representing two straight lines that are either parallel or intersecting at z_g. It is easy to see that these are perpendicular to the line connecting the charged electrodes at the point z_m for $v(z_\mathrm{p}^*) = 0$ and z_p for $v(z_\mathrm{m}^*) = 0$ respectively. This observation is central to the development of our algorithm and we formalise it in the form of the next theorem.

Theorem V.1. *If $D_{\mathrm{p}^o(z_\mathrm{g})}(z)$ is the dipole potential approximation of the potential $v_o(z)$ induced by the polarisation of a disk-shaped inclusion Ω centred at $z_\mathrm{g} \in \mathcal{C}$ such that $|z - z_\mathrm{g}| \to \infty$, and $z_\mathrm{p},\, z_\mathrm{m} \in \mathcal{S}^t$ are the coordinates of the positively and negatively charged electrodes then if there is a point z_p^* such that $D_{\mathrm{p}^o(z_\mathrm{g})}(z_\mathrm{p}^*) = 0$ then the condition $\langle z_\mathrm{g} - z_\mathrm{m}, z_\mathrm{m} - z_\mathrm{p}^* \rangle = 0$ holds. Similarly, if there is a point z_m^* such that $D_{\mathrm{p}^o(z_\mathrm{g})}(z_\mathrm{m}^*) = 0$, then $\langle z_\mathrm{g} - z_\mathrm{p},\, z_\mathrm{p} - z_\mathrm{m}^* \rangle = 0$ holds true.*

Proof. Developing the inner product in (47) yields

$$|\bar{z}_\mathrm{gp}|^2 - \frac{|z_\mathrm{gp}|}{|z_\mathrm{gm}|}\big\langle \bar{z}_\mathrm{gp}, \bar{z}_\mathrm{gm} \big\rangle = 0$$

hence since $\bar{z}_\mathrm{gp}$ is unit,

$$\frac{|z_\mathrm{gp}|}{|z_\mathrm{gm}|}\big\langle \bar{z}_\mathrm{gp}, \bar{z}_\mathrm{gm} \big\rangle = 1.$$

Utilizing $\big\langle z_\mathrm{gp}, z_\mathrm{gm} \big\rangle = |z_\mathrm{gp}||z_\mathrm{gm}|\big\langle \bar{z}_\mathrm{gp}, \bar{z}_\mathrm{gm} \big\rangle$ the above becomes

$$\frac{1}{|z_\mathrm{gm}|^2}\big\langle z_\mathrm{gp}, z_\mathrm{gm} \big\rangle = 1.$$

Let $z_\mathrm{mp} = z_\mathrm{m} - z_\mathrm{p}$ such that $z_\mathrm{mp} = z_\mathrm{gp} - z_\mathrm{gm}$. Introducing to the above yields

$$\begin{aligned}
\frac{1}{|z_\mathrm{gm}|^2}\big\langle z_\mathrm{gp}, z_\mathrm{gm} \big\rangle &= 1 \\
\frac{1}{|z_\mathrm{gm}|^2}\big\langle z_\mathrm{mp} + z_\mathrm{gm}, z_\mathrm{gm} \big\rangle &= 1 \\
\frac{1}{|z_\mathrm{gm}|^2}\Big(\big\langle z_\mathrm{mp}, z_\mathrm{gm} \big\rangle + \big\langle z_\mathrm{gm}, z_\mathrm{gm} \big\rangle\Big) &= 1 \\
\frac{1}{|z_\mathrm{gm}|^2}\big\langle z_\mathrm{mp}, z_\mathrm{gm} \big\rangle &= 0
\end{aligned}$$

Since $|z_\mathrm{m} - z_\mathrm{g}| \neq 0$ at the far field, the above is true only when $\big\langle z_\mathrm{mp}, z_\mathrm{gm} \big\rangle = 0$, which proves the required relation. The case for $\langle z_\mathrm{g} - z_\mathrm{p},\, z_\mathrm{p} - z_\mathrm{m}^* \rangle = 0$ follows similarly. □

These criteria are graphically illustrated in figure 4, showing that at z_p^* or z_m^* the current injecting electrodes and the geometric centre of the inclusion z_g are at the vertices of a right-angle triangle. Moreover, notice that the vector z_mp is defined by the coordinates of the two charged electrodes, irrespectively of the curvature of the cable.

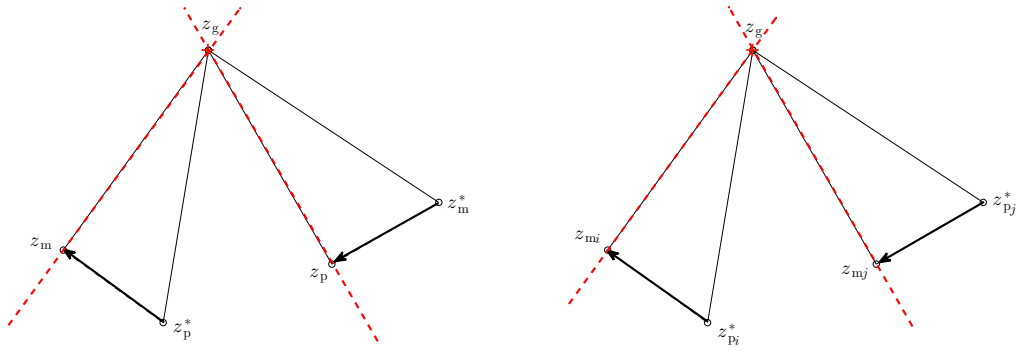

Fig. 4. For the figure at the left, the conditions where $D_{\mathrm{p}^o(z_{\mathrm{g}})}(z^*_{\mathrm{p}}) = 0$ and $D_{\mathrm{p}^o(z_{\mathrm{g}})}(z^*_{\mathrm{m}}) = 0$ are satisfied, signify that the charged electrodes and the centre of the inclusion are at the vertices of some right angle triangles. Notice the right angles at z_{m} and z_{p} respectively. For the pair of triangles to the right, the equivalent conditions for $D_{\mathrm{p}^o(z_{\mathrm{g}})}(z^*_{\mathrm{p}i}) = 0$ and $D_{\mathrm{p}^o(z_{\mathrm{g}})}(z^*_{\mathrm{p}j}) = 0$.

From a practical prospective, establishing a pair $(z^*_{\mathrm{p}}, z^*_{\mathrm{m}})$ so that to yield the necessary lines intersecting at the inclusion can become difficult, since even if one measures a zero polarisation potential at one of the injecting electrodes, this does not guarantee a subsequent zero at the other pole soon after. To circumvent this problem suppose that at time t, a measurement $v(z^*_{\mathrm{p}_i}) = 0$ is obtained while the array is towed along some predefined survey trajectory. At the same time let the corresponding negative electrode be positioned at $z_{\mathrm{m}_i} \in \mathcal{S}^t$. Suppose now that the towing vessel executes a 2π turn of circumference that is bigger than the length of the cable, starting and ending near $z^*_{\mathrm{p}_i}$. This manoeuvre is likely to yield another pair of points at $z_{\mathrm{p}^*_j}$ and z_{m_j}. In this case the two lines intersecting at the centre of the inclusion are

$$\begin{cases} \langle z_{\mathrm{g}} - z_{\mathrm{m}_i}, z_{\mathrm{m}_i} - z^*_{\mathrm{p}_i} \rangle &= 0, \\ \langle z_{\mathrm{g}} - z_{\mathrm{m}_j}, z_{\mathrm{m}_j} - z^*_{\mathrm{p}_j} \rangle &= 0, \end{cases} \tag{49}$$

and the geometric arrangement of the points is similar to the previous case as depicted in figure 4. The first equation is the line normal to the vector $z_{\mathrm{m}_i} - z^*_{\mathrm{p}_i}$ passing through z_{m_i} while the second is the line normal to $z_{\mathrm{m}_j} - z^*_{\mathrm{p}_j}$ at z_{m_j}. The procedure for when encountering $v(z^*_{\mathrm{m}_i}) = 0$ first follows

similarly with the relevant equations changed to

$$\begin{cases} \langle z_{\rm g} - z_{{\rm p}_i}, z_{{\rm p}_i} - z^*_{{\rm m}_i} \rangle &= 0, \\ \langle z_{\rm g} - z_{{\rm p}_j}, z_{{\rm p}_j} - z^*_{{\rm m}_j} \rangle &= 0. \end{cases} \tag{50}$$

Assuming that the ocean current disturbances have a small impact on the displacement of the cable, let the cable be towed on a circular trajectory C_R of radius $R > l/2\pi$, such that C_R overlays $\mathcal{S}^t$ with $|z_{\rm p} - z_{\rm m}| < l$. As $z_{\rm p}$ completes a 2π turn, the line orthogonal to the distance vector $z_{\rm p} - z_{\rm m}$ at $z_{\rm m}$, rotates tangentially to the periphery of a smaller, concentric circle c_r whose diameter scales to the distance $|z_{\rm p} - z_{\rm m}|$. This manoeuvre is aimed to yielding a second zero polarisation potential measurement irrespectively of the direction of the turn. If the cable moves on C_R without being displaced by sea currents, then a zero crossing is certain, unless $z_{\rm g}$ is situated within a region comprising the inner circle c_r or a small region adjacent to C_R (see for example figure 5). In such case the inclusion remains undetectable through this scheme, however given the proximity of c_r to the array it is likely that the inclusion will be detected by the large variation in the electrical potential measurements instead. The main steps of the algorithm for localising the centre of an inclusion are:

Note that the algorithm does not require excessive data acquisition or storage, as the localisation of the inclusion ultimately requires solving a 2×2 linear system. On the other hand, the induced potential measurements are substantially weaker than the imposed ones, and therefore extracting the time series $v(z_{\rm p}, t)$ from $u(z_{\rm p}, t)$ becomes challenging in the presence of noise. Nonetheless, even without additive noise, the algorithm will encounter some systematic sources of errors, primarily due to the dipole approximation of the polarisation potential that also incorporates the circular shape regularity assumption. A further complication arises by the fact that the required $z^*_{\rm p}$ and $z^*_{\rm m}$ are not likely to be sampled directly, but rather estimated from adjacent measurements of opposite polarity. Moreover, although addressed by assumption 1, one has to consider what happens when the measured polarisation potential arises not by one, but various distinct inclusions that happen to be in the vicinity of the measurement. Indeed, the case of multiple inclusions poses the challenge of identifying which pairs

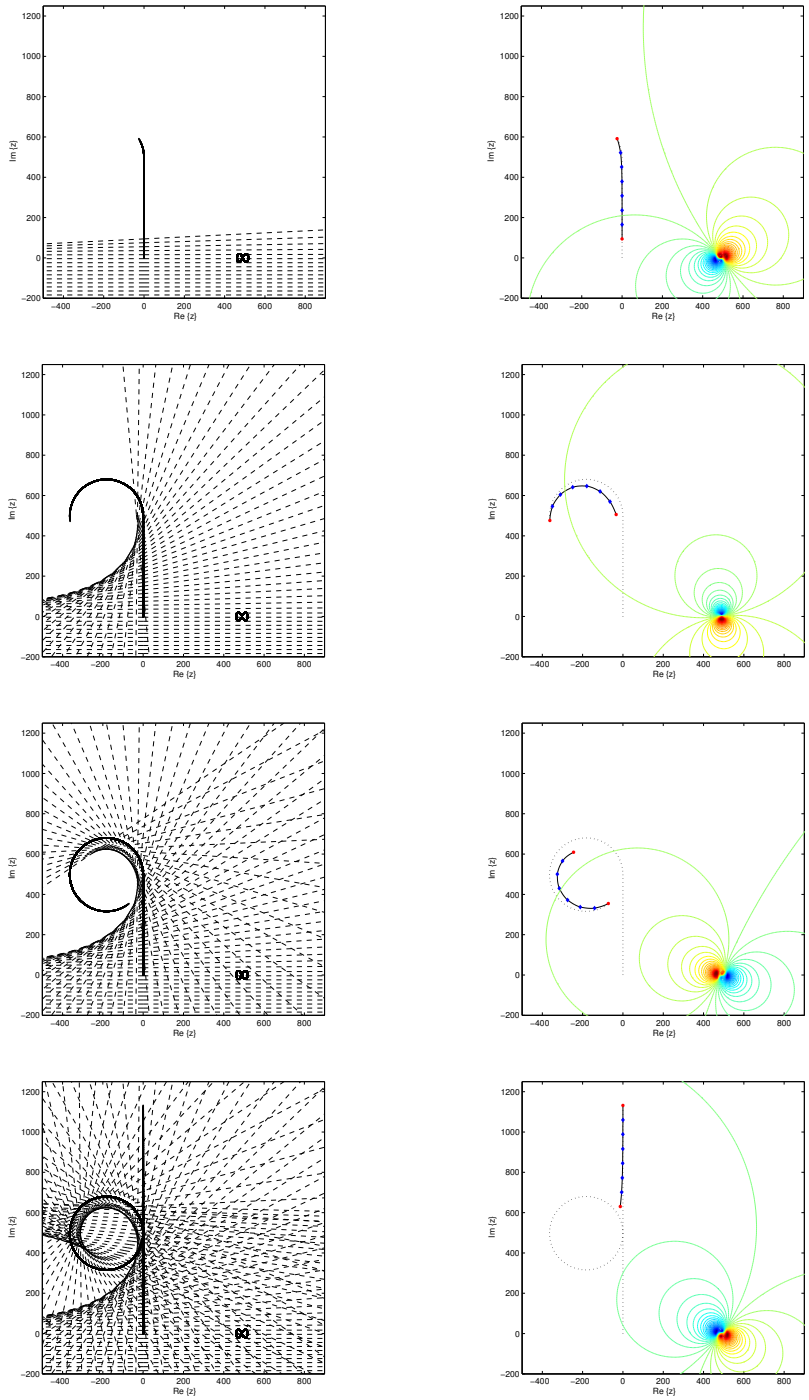

Fig. 5. The C_R manoeuvre to establish a second zero in the polarisation induced potential. In the right column there are four snapshots of the 500 m long electric array as it performs a complete turn with a radius of about 180 m, and the corresponding polarisation potential due to an inclusion situated at the bottom right. The figures on the left column, show the (dashed) lines that are normal to line connecting the active electrodes (red dots) as the cable is changing its position. The inclusion becomes detectable if it resides in a region where two or more lines are intersecting. At the last row notice the region in the interior and the left of C_R that does not contain any line crossings. Any inclusions situated therein remain detectable under this scheme.

Algorithm 1 Detecting and localising the centre of an inclusion $z_{\rm g}$ from $v(z_{\rm p},t)$

Ensure: At $t=0$ initiate the survey by towing the array on a predefined trajectory with constant velocity τ

for $t \leftarrow t+\delta t$ **do**

Move the cable to new position $\mathcal{S}^t$,

Apply current f,

Simulate/measure $u(z_{\rm p},t)$,

Compute $v(z_{\rm p},t)=u(z_{\rm p},t)-u^h(z_{\rm p},t)$,

if $\mathrm{sgn}(v(z_{\rm p},t)) \neq \mathrm{sgn}(v(z_{\rm p},t-\delta t))$ **then**

Perform manoeuvre C_R

end if

end for

De-noise the time series $v(z_{\rm p})$,

Identify the points where $v({z_{\rm p}}_i^*)=0$ and $v({z_{\rm p}}_j^*)=0$,

Identify the zero-crossing coordinates $\{{z_{\rm p}}_i^*, z_{{\rm m}i}\}$ and $\{{z_{\rm p}}_j^*, z_{{\rm m}j}\}$,

Solve a 2×2 linear system to obtain $z_{\rm g}$.

of lines correspond to each inclusion? As we demonstrate in the numerical results section, we process the points $\{(z_{{\rm p}_i}^*, z_{{\rm m}_i})\}_{i=1}^n$ sequentially, computing a number of plausible $z_{\rm g}$ points, anticipating that these will concentrate around the true inclusion centres.

VI. Error Analysis

In this section we address the sensitivity of the localisation algorithm to additive noise and default inaccuracies in positioning data and electric measurements. Recall that the zero polarisation potential coordinates $z_{\rm p}^*$, $z_{\rm m}^*$ are unlikely to be sensed directly, but rather estimated from nearby points where subsequent polarisation data change in polarity. Consider for example the linear system arising from

the two line equations in (49) and let us normalise the vectors to

$$\bar{z}_{\mathrm{mp}_i} = \frac{z_{\mathrm{m}_i} - {z_{\mathrm{p}_i}}^*}{|z_{\mathrm{m}_i} - {z_{\mathrm{p}_i}}^*|}, \quad \bar{z}_{\mathrm{mp}_j} = \frac{z_{\mathrm{m}_j} - {z_{\mathrm{p}_j}}^*}{|z_{\mathrm{m}_j} - {z_{\mathrm{p}_j}}^*|},$$

so that the two line equations are compactly expressed as

$$\langle z - z_{\mathrm{m}_i}, \bar{z}_{\mathrm{mp}_i} \rangle = 0, \quad \langle z - z_{\mathrm{m}_j}, \bar{z}_{\mathrm{mp}_j} \rangle = 0.$$

Considering the errors in the measurements we can pose the problem of finding where these lines cross as a least squares problem. Effectively, squaring the distance of a point z from either line and then adding together yields

$$S(z) = (z - z_{\mathrm{m}_i})' \bar{z}_{\mathrm{mp}_i} \otimes \bar{z}_{\mathrm{mp}_i} (z - z_{\mathrm{m}_i}) + (z - z_{\mathrm{m}_j})' \bar{z}_{\mathrm{mp}_j} \otimes \bar{z}_{\mathrm{mp}_j} (z - z_{\mathrm{m}_j}),$$

where $\otimes$ is the exterior vector product on $\mathcal{C}$. Upon setting the gradient of the above to zero we obtain

$$\mathbf{A}\, z_{\mathrm{g}} = b \tag{51}$$

where

$$\mathbf{A} = \bar{z}_{\mathrm{mp}_i} \otimes \bar{z}_{\mathrm{mp}_i} + \bar{z}_{\mathrm{mp}_j} \otimes \bar{z}_{\mathrm{mp}_j}, \text{ and} \tag{52}$$

$$b = (\bar{z}_{\mathrm{mp}_i} \otimes \bar{z}_{\mathrm{mp}_i}) z_{\mathrm{m}_i} + (\bar{z}_{\mathrm{mp}_j} \otimes \bar{z}_{\mathrm{mp}_j}) z_{\mathrm{m}_j}. \tag{53}$$

If the errors are small enough such that $\|\delta\mathbf{A}\| < \|\mathbf{A}\|$ and $\|\delta b\| < \|b\|$, then subtracting the exact system (51) from the perturbed $(\mathbf{A} + \delta\mathbf{A})(z_{\mathrm{g}} + \delta z_{\mathrm{g}}) = (b + \delta b)$, yields the localisation error in analytic form

$$\delta z_{\mathrm{g}} = (\mathbf{I} + \mathbf{A}^{-1}\delta\mathbf{A})^{-1}\mathbf{A}(\delta b - \delta\mathbf{A} z_{\mathrm{g}}). \tag{54}$$

Based on perturbation theory [26], if $\|\mathbf{A}^{-1}\delta\mathbf{A}\| < 1$ then the relative error in the solution can be shown to be bounded by

$$\frac{\|\delta z_{\mathrm{g}}\|}{\|z_{\mathrm{g}}\|} \leq \mathrm{cond}(\mathbf{A}) \left(\frac{\|\delta\mathbf{A}\|}{\|\mathbf{A}\|} + \frac{\|\delta b\|}{\|b\|} \right), \tag{55}$$

noting briefly that a tighter bound can be obtained by exploiting the particular structure of the errors in $\mathbf{A}$ and b in an element-wise basis such as $|\delta a_{ij}| \leq \epsilon$, if such information is available. From (55) it

is evident that the localisation error scales proportionally to the condition number of $\mathbf{A}$, but further to that we ask how can this result be utilised to improve the performance, e.g. stability, of the method. In other words, what does this error bound tell us about the way that data are acquired? Recall the definition

$$\mathbf{A} = \bar{z}_{\mathrm{mp}_i} \otimes \bar{z}_{\mathrm{mp}_i} + \bar{z}_{\mathrm{mp}_j} \otimes \bar{z}_{\mathrm{mp}_j},$$

let ψ be the angle between the unit vectors $\bar{z}_{\mathrm{mp}_i}$ and $\bar{z}_{\mathrm{mp}_j}$. Notice that $\mathbf{A}$ is the sum of two rank-1 symmetric matrices. In this setting some limiting cases are readily observable, for example when $\psi = \pi/2$ or $3\pi/2$ then $\langle \bar{z}_{\mathrm{mp}_i}, \bar{z}_{\mathrm{mp}_j} \rangle = 0$, and thus $\mathbf{A}$ is orthogonal with eigenvectors $\bar{z}_{\mathrm{mp}_i}$ and $\bar{z}_{\mathrm{mp}_j}$ and a double eigenvalue equal to one. In this case the matrix attains a condition number of one, and thus we anticipate the estimate of z_{g} to be robust against the errors. On the other hand, if $\psi = 0$ or $\psi = \pi$, then $\bar{z}_{\mathrm{mp}_i}$ and $\bar{z}_{\mathrm{mp}_j}$ are collinear or parallel and thus $\mathbf{A}$ will have one non-zero eigenvalue, and thus a very large condition number. In the general case, as we sketch in the appendix,

$$\mathrm{cond}(\mathbf{A}) = \begin{cases} |\cot(\psi/2)| & \text{if } \cos\psi \geq 0 \\ |\tan(\psi/2)| & \text{if } \cos\psi < 0, \end{cases} \tag{56}$$

affirming that data $(z^*_{\mathrm{p}_i}, z_{\mathrm{m}_i})$ and $(z^*_{\mathrm{p}_j}, z_{\mathrm{m}_j})$ obtained at $\mathcal{S}^i$ and $\mathcal{S}^j$ respectively yield a robust estimate of z_{g} if the lines connecting the charged electrodes in their respective cable orientations are close to being orthogonal.

VII. Filtering the data

Instead of forming and solving the system (51) directly using the noisy data, it may be advantageous to apply some noise filtering beforehand. The inherent smoothness of the polarisation measurements $z_{\mathrm{p}}(t)$ or $z_{\mathrm{m}}(t)$ can be exploited to de-noise the data without a significant compromise in the signal. Consider the noise model of the measurements

$$v(z_{\mathrm{p}}, t) = u(z_{\mathrm{p}}, t) - u^h(z_{\mathrm{p}}, t) + \eta, \quad z_{\mathrm{p}} \in \mathcal{S}^t,\ t \in [0, t_1, \ldots, t_{\mathrm{end}}], \tag{57}$$

where η is the additive random noise, then we require that for $|\eta| \to 0$, $v(z_{\rm p}, t)$ is sufficiently smooth. This remark is formalised in the form of the next theorem.

Theorem VII.1. *Let $v(z_{\rm p}), v(z_{\rm m})$ the induced potential at injecting electrodes $z_{\rm p}, z_{\rm m}$, consider a time $t_{\rm end} > 0$ and suppose that $z_{\rm p}, z_{\rm m} \in C^n([0, t_{\rm end}], \mathcal{C} \setminus \overline{\Omega})$ for $n \geq 0$, then $v(z_{\rm p}, t), v(z_{\rm m}, t) \in C^n([0, t_{\rm end}], \Re)$.*

Proof. Recalling that

$$u^h(z) = \frac{i_f}{\sigma_h}\big[\Phi(z - z_{\rm p}) - \Phi(z - z_{\rm m})\big] \ , \ z \in \mathcal{C} \setminus \{z_{\rm p}, z_{\rm m}\},$$

where i_f is the magnitude of the applied current and Φ is the fundamental solution of the Laplace equation

$$\Phi(z - z') = \frac{1}{2\pi} \ln \frac{1}{|z - z'|} \ , \ z \neq z'.$$

It is obvious that $t \mapsto \partial\Phi_{\nu(z)}(z - z_{\rm p}(t))$ and $t \mapsto \partial\Phi_{\nu(z)}(z - z_{\rm m}(t))$ are C^n functions from $[0, t_{\rm end}]$ to $H^{-1/2}(\partial\Omega)$, hence $\partial_\nu u^h \in C^n([0, t_{\rm end}], H^{-1/2}(\partial\Omega))$. In fact, since none of the active electrodes is in $\overline{\Omega}$, we have $\partial_\nu u^h \in C^n([0, t_{\rm end}], H_\diamond^{-1/2}(\partial\Omega))$. Moreover, $(\mathbf{I} - \mu\mathbf{K}')^{-1}$ is a bounded linear operator of $H_\diamond^{-1/2}(\partial\Omega)$ and $t \mapsto \Phi(z - z_{\rm p}(t))$ and $t \mapsto \Phi(z - z_{\rm m}(t))$ are C^n functions from $[0, t_{\rm end}]$ to $H^{1/2}(\partial\Omega)$. Since

$$v(z_{\rm p}, t) = 2\mu \int_{\partial\Omega} \Phi(z - z_{\rm p}(t)) \left((\mathbf{I} - \mu\mathbf{K}')^{-1}\partial_\nu u^h(t)\right)(z)\, {\rm d}s(z) \ , \ t \in [0, t_{\rm end}]$$

and

$$v(z_{\rm m}, t) = 2\mu \int_{\partial\Omega} \Phi(z - z_{\rm m}(t)) \left((\mathbf{I} - \mu\mathbf{K}')^{-1}\partial_\nu u^h(t)\right)(z)\, {\rm d}s(z) \ , \ t \in [0, t_{\rm end}],$$

we have $v(z_{\rm p}, t), v(z_{\rm m}, t) \in C^n([0, t_{\rm end}], \Re)$. □

In order to estimate the exact $v(z_{\rm p}, t)$ from the measurements under these extreme noise conditions, suppose that at time t we sample the potential field s times on each active electrode, for example $\{u^{(1)}(z_{\rm p}, t), \ldots, u^{(s)}(z_{\rm p}, t)\}$, from where the induced potential samples $\{v^{(1)}(z_{\rm p}, t), \ldots, v^{(s)}(z_{\rm p}, t)\}$ can be extracted. Since both u and v contain the same noise the s-sample based average measurement

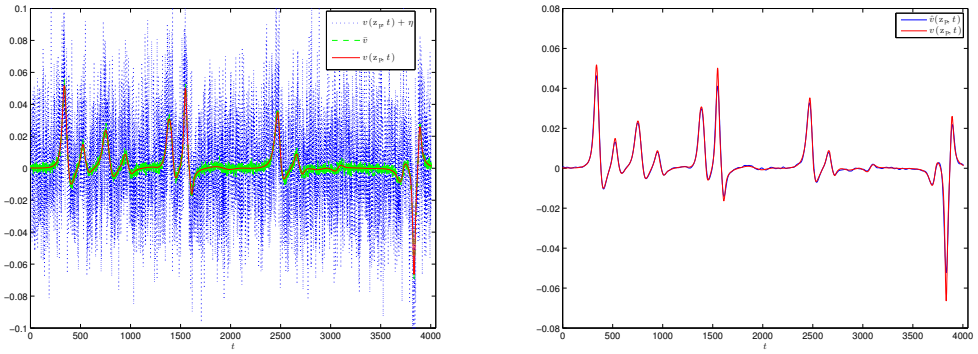

Fig. 6. At the left, the true (red) and noise infused (blue) polarisation potential data at z_{p}, and to the right the estimated de-noised time series data for $v(z_{\mathrm{p}})$ using the smooth regularisation filter approach.

at time t is $\bar{v}_t = \frac{1}{s}\sum_{i=1}^{s} v^{(i)}(z_{\mathrm{p}}, t)$, and let $\bar{v} \in \Re^{N_t}$ the vector of averaged polarisation potentials over N_t time instants. Further let $\mathbf{S} \in \Re^{N_t \times N_t}$ be a discrete, smoothness-imposing regularisation operator [27], then an estimator of v can be obtained by solving

$$\hat{v} = \arg\min_{v \in \Re^{N_t}} \left\{ \left\| \bar{v} - v \right\|^2_{\mathbf{\Sigma}_\eta^{-1}} + \left\| \mathbf{S}\, v \right\|^2 \right\}, \tag{58}$$

where $\mathbf{\Sigma}_\eta \in \Re^{N_t \times N_t}$ is the sample-based noise covariance of the data, in this case a diagonal matrix. This problem has an analytic solution

$$\hat{v} = \left(\mathbf{S} + \mathbf{\Sigma}_\eta^{-1} \right)^{-1} \mathbf{\Sigma}_\eta^{-1} \bar{v}. \tag{59}$$

In addition to the smoothness of the time series $v(z_{\mathrm{p}}, t)$ and $v(z_{\mathrm{m}}, t)$ one may also opt to exploit the smoothness of the polarisation potential profile on $\mathcal{S}^t$ by considering the measurements on electrodes adjacent to z_{p} and z_{m}. The graphs in figure 6 show a simulated time series of polarisation measurements infused with Gaussian noise of variance equal to 5% of the recorded total potential $u(z_{\mathrm{p}})$, the polarisation data sample-averages $\bar{v}$, and the de-noised signal $v(z_{\mathrm{p}})$.

VIII. Numerical Results

In this section we present some numerical results aimed at testing the performance of our algorithm. We consider a domain with uniform background conductivity of $\sigma_h = 1$ S/m, in which we position three small inclusions centred at $z_{\mathrm{g}_1} = 150 + 1350\mathrm{i}$, $z_{\mathrm{g}_2} = 805$, and $z_{\mathrm{g}_3} = 1850 + 625\mathrm{i}$ as shown in figure 7. The simulation of the measurements involves a 200 m long electrical array of 0.0225 m in diameter, towed at a constant speed of 2 m/s. The array is equipped with eight equidistant point electrodes, including the pair that applies the currents at front and rear ends of the cable respectively, through which a direct current of 20 A was applied every two seconds. To the simulated data a zero-mean white Gaussian noise was added at a standard deviation of 5% of the recorded $u(z_{\mathrm{p}}, t)$ measurement, noting that this was in the region of 30 V. For each measurement 300 samples have been simulated from where the sample mean and variance are estimated. This data acquisition rate is well within reach using state-of-the-art instrumentation, under a single current pattern excitation [28]. Subsequently these data were smoothed using a second-order discrete gradient operator as in (58). The zero-crossing points are estimated by averaging the coordinates of the two consecutive polarisation potential measurements of opposite polarity. The vessel is set to perform data acquisition on a predefined trajectory where it comes under the influence of time-varying ocean currents with amplitude no bigger than 2 m/s. As the electric potentials are sampled at z_{p} and z_{m}, when a polarity change in the measurements $v(z_{\mathrm{p}})$ is recorded then the vessel may opt to perform a full turn manoeuvre, with the direction of the turn chosen arbitrarily. To solve the forward problem, the integral equation (23) was solved numerically on a grid with 0.5 m resolution.

In the first test we assume that the inclusions have conductivity values $\sigma_1 = 10^{-3}$, $\sigma_2 = 10^{-1}$, and $\sigma_3 = 10^2$ S/m. As shown in the left figure in 7, a total of six manoeuvres were performed triggered by zero-crossings in the filtered time-series $\hat{v}(z_{\mathrm{p}})$. The simulation yielded a time series of 4007 data for $v(z_{\mathrm{p}})$ and $v(z_{\mathrm{m}})$, from where a total of 75 zero-crossings have been resolved after the de-noising process, compared to 51 in the exact data. The overall duration of the survey was about 2.2 h, covering

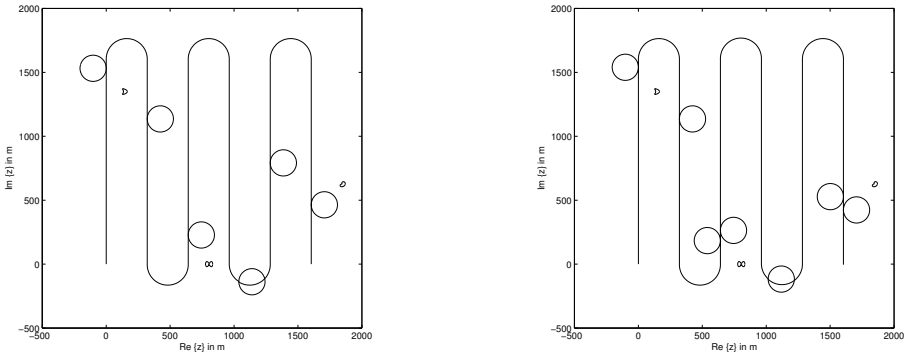

Fig. 7. Two simulated survey trajectories used in the numerical simulation tests, with six and seven manoeuvres respectively. The figures indicate also the three targeted inhomogeneities.

an area of about 6 Km^2. The localisation results of this simulation are plotted in figure 9. To the left the processing of the linear systems (51) considering all $v(z_{\mathrm{p}}^*) = 0$ and $v(z_{\mathrm{m}}^*) = 0$ points without any additive noise, allowing only the default positioning errors due to the estimation of z_{p}^* and z_{m}^*. The results show a good concentration of the estimated z_{g} points in the vicinity of the three inclusions, however there are a few isolated prediction points away from them. These 'ghost points' are caused by pairing zero polarisation data points that correspond to different inclusions. Note that although it is easy to work out the intersection of lines arising from the same inhomogeneity, this task is no longer trivial when having several such inclusions. To the right of the same figure we plot the corresponding results after infusing the noise signal into the measurements. In this case, we notice some dispersion among the estimators, although arguably these maintain a reasonable clustering around the targets. In both cases the leftmost inclusion is localised the best and the rightmost the worst, however it must also be noted that the later was only sensed from one side.

To investigate the impact of conductivity contrast on the performance of the algorithm, we repeat the simulation for the same inclusions but we interchange their values to $\sigma_1 = 10^{-1}$, $\sigma_2 = 10^2$, and $\sigma_3 = 10^{-3}$ S/m. This time the survey trajectory ended up including seven manoeuvres yielding a total

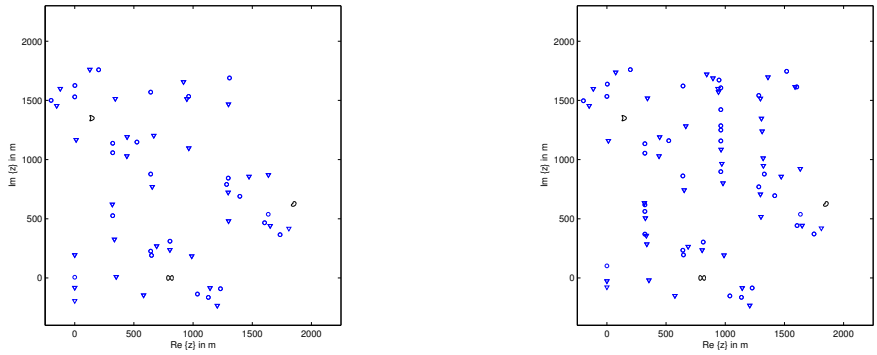

Fig. 8. The filtered data for the first simulation test with and without additive noise. The $\circ$ correspond to the estimated z_{p}^{*} coordinates, the $\triangledown$ to the estimated z_{m}^{*} coordinates. The figure on the left is without the additive noise, and that on the right is with 5% zero-mean Gaussian noise. The values of the inhomogeneities from left to right are 0.001, 0.1 and 100 S/m in a conductivity background of 1 S/m.

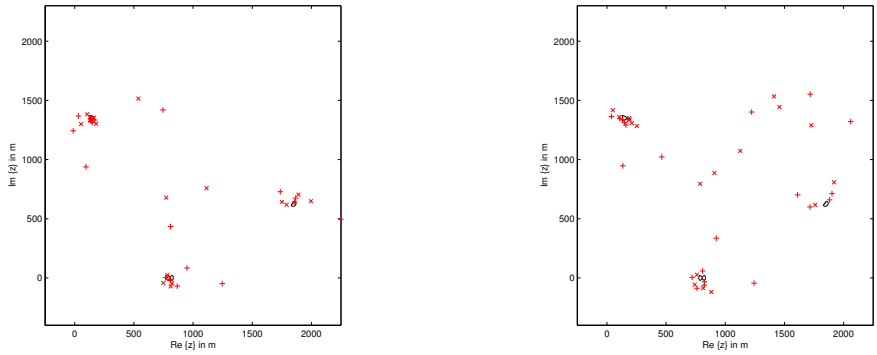

Fig. 9. The results for the first simulation test with and without additive noise. The $\times$ and $+$ are the z_{g} estimators from z_{p}^{*} and z_{m}^{*} respectively. The figure on the left is without the additive noise, and that on the right is with 5% zero-mean Gaussian noise. The values of the inhomogeneities from left to right are 0.001, 0.1 and 100 S/m in a conductivity background of 1 S/m.

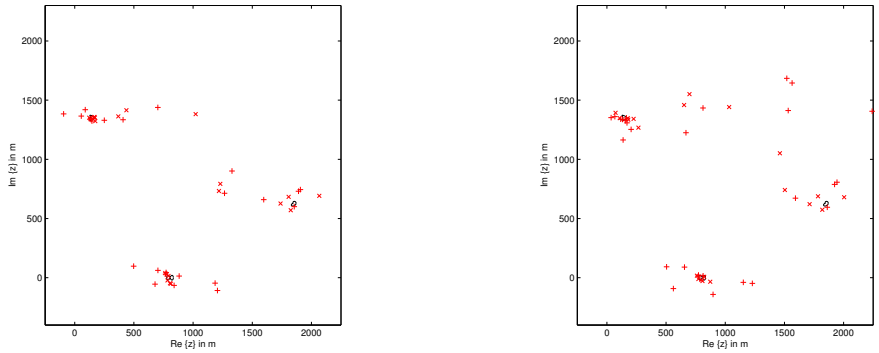

Fig. 10. The results for the second simulation test with and without additive noise. The $\times$ and $+$ are the z_{g} estimators from z_{p}^{*} and z_{m}^{*} respectively. The figure on the left is without the additive noise, and that on the right is with 5% zero-mean Gaussian noise. This figure is similar to 9 except the values of the inhomogeneities from left to right were changed to 0.1, 100 and 0.001 S/m in a conductivity background of 1 S/m.

of 4169 measurements for for $v(z_{\mathrm{p}})$ and $v(z_{\mathrm{m}})$, lasting about 2.3 h. Among them from where a total 77 zero-crossings have been resolved after the de-noising process, compared to 55 in the noise-free data. The measurements were subsequently infused with zero-mean Gaussian noise just like the previous case, and the results from the algorithm are illustrated in figure 10. Comparing with the previous test, it is apparent that the impact of additive noise in the performance of the algorithm is sustained, but we observe no significant variation in the results with respect to the change of conductivity values.

A. Model limitations and extensions

The 2D model used in this study is based on the depth-averaged bulk conductivity of the 3D domain. In this context the third dimension is incorporated into the 2D model through the integral of the conductivity profile along the third dimension. This projection is clearly not unique, and thus our method cannot resolve the z coordinate of the inclusion. In general, the polarisation potentials of 3D inclusions will differ from those considered here even if those are situated close to the horizontal plane. However, as the current injecting electrodes are always on the plane, if the inclusions are assumed to be

spherical and close to the surface then their equivalent electric dipoles will have moments predominantly aligned to the plane. As the inclusion moves to a higher depth then the vertical component of the dipole moment will increase and the 2D model approximation will no longer be valid. In effect, the 2D model is more appropriate to small 3D inclusions when these are close to the surface.

The measurements of electric potential are sensitive to the depth-averaged bulk conductivity as defined in (1). The proposed framework is thus appropriate for localising depth-invariant inhomogeneities of small diameter as well as small discrete inclusions situated near the surface as long as their conductivity value provides an adequate contrast to the bulk conductivity of the background medium. In this context the methodology is suitable for detecting submarine groundwater discharge, considering the small volume of the flow and the high contrast in electric conductivity between spring water and seawater [29]. Previous studies on this topic have utilised towed electrical tomography in conjunction with chemical analysis sampling in order to delineate the aquifer and image the fluid interactions [30].

This work can be viewed as a step toward a more realistic 3D model and inversion scheme. In regards to the forward problem the extension appears to be obvious, but the localisation problem has some complications. In principle, the integral equation (23) for the polarisation density can be formulated in three dimensions and then the effective dipole approximation can be applied by assuming spherical inclusions, using the framework in [10]. The imposed potential will be adapted according to the Green's function for the Laplacian equation in 3D, the criteria on the measured polarisation potential will remain as in theorem IV.1, only this time one should be looking for the equations of three crossing planes. However, if the zero-crossing coordinates z_{p}^{*} and z_{m}^{*} are restricted to the horizontal plane then the vertical coordinate of the inclusion's centre cannot be resolved, as the intersecting planes will all be orthogonal to the horizontal. This indicates the need to measure the potential at various different depths, which in turn implies towing the electrical array on a 3D trajectory.

IX. Conclusions

We have addressed the problem of detecting and localising a small number of inhomogeneities immersed in the homogeneous open plane, using towed electrical sensing. Assuming these are dispersed away from each other, we have modelled the measurement using an electromechanical system based on the single layer potential formulation. We have showed that sampling the potential induced by the polarisation of these inclusions at the current injecting electrodes yields sufficient information to locate them without knowing their conductivity values or shapes. In particular, subject to an a priori assumption on the shape of the inclusions, the far-field polarisation potential can be approximated to second-order accuracy to a dipole potential. Using this approximation we have proposed an algorithm based on a geometric criterion that a zero polarisation measurement at a charged electrode requires the two charged electrodes and the centre of the inclusion to be at the vertices of a right angle triangle. The performance of the proposed methodology has been assessed using error analysis and numerical simulation. The results indicate that the algorithm maintains a fair robustness to data noise and has a low computational implementation cost.

Appendix

Using the trigonometric identity $\tan(\psi/2) = \pm\sqrt{\frac{1-\cos\psi}{1+\cos\psi}}$, to show that

$$\operatorname{cond}(\mathbf{A}) = \begin{cases} |\cot(\psi/2)| & \text{if } \cos\psi \geq 0 \\ |\tan(\psi/2)| & \text{if } \cos\psi < 0, \end{cases}$$

is equivalent to showing

$$\operatorname{cond}(\mathbf{A}) = \sqrt{\frac{1+\cos\psi}{1-\cos\psi}} \quad \text{if } \cos\psi \geq 0 \quad \text{and} \quad \sqrt{\frac{1-\cos\psi}{1+\cos\psi}} \quad \text{if } \cos\psi < 0.$$

For the later it suffices to prove that the two eigenvalues of $\mathbf{A}$ are $\lambda_1 = (1-\cos\psi)$ and $\lambda_2 = (1+\cos\psi)$ where $\cos\psi = \langle \bar{z}_{\mathrm{mp}_i}, \bar{z}_{\mathrm{mp}_j} \rangle$. Recall the definition of the matrix as a sum of exterior products

$$\mathbf{A} = \bar{z}_{\mathrm{mp}_i} \otimes \bar{z}_{\mathrm{mp}_i} + \bar{z}_{\mathrm{mp}_j} \otimes \bar{z}_{\mathrm{mp}_j},$$

hence if $\langle \bar{z}_{\mathrm{mp}_i}, \bar{z}_{\mathrm{mp}_j} \rangle = 0$ then $\bar{z}_{\mathrm{mp}_i}$ and $\bar{z}_{\mathrm{mp}_j}$ are the two eigenvectors of the matrix with corresponding eigenvalues $\lambda_1 = \lambda_2 = 1$. If these are not orthogonal then there exists a new orthogonal basis of two vectors such that the sum of their individual exterior products is equal to $\mathbf{A}$. Let the phasor definitions of the two unit vectors as $\bar{z}_{\mathrm{mp}_i} = e^{\mathrm{i}\psi_i}, \bar{z}_{\mathrm{mp}_j} = e^{\mathrm{i}\psi_j}$ then the entries of the matrix become

$$\mathbf{A} = \begin{pmatrix} \cos^2\psi_i + \cos^2\psi_j & \cos\psi_i \sin\psi_i + \cos\psi_j \sin\psi_j \\ \cos\psi_i \sin\psi_i + \cos\psi_j \sin\psi_j & \sin^2\psi_i + \sin^2\psi_j \end{pmatrix}$$

Taking the trace and the determinant of the 2×2 matrix gives

$$\mathrm{Tr}(\mathbf{A}) = \lambda_1\lambda_2 = 2, \quad |\mathbf{A}| = \lambda_1\lambda_2 = \sin^2(\psi_i - \psi_j).$$

Using the fact that $\psi = \psi_i - \psi_j$ and the identity $\lambda_1\lambda_2 = (1 - \cos^2\psi)$ we obtain the required result. To locate the corresponding eigenvectors we first form the unit vector $z_k = (\bar{z}_{\mathrm{mp}_i} + \bar{z}_{\mathrm{mp}_j})/|\bar{z}_{\mathrm{mp}_i} + \bar{z}_{\mathrm{mp}_j}|$ and then $z_1 = R_\perp z_k$ and $z_2 = R_\perp z_1$ where $R_\perp$ is the orthogonal anti-clockwise rotation operator, thus $\mathbf{A} = \lambda_1 z_1 \otimes z_1 + \lambda_2 z_2 \otimes z_2$.

REFERENCES

[1] S. Passaro, "Marine electrical resistivity tomography for shipwreck detection in very shallow water: a case study from agropoli (salerno, southern italy)," *Journal of Archaeological Science*, vol. 37, pp. 1989–1998, 2010.

[2] F. D. D. Lewis, E. A. White, C. D. Johnson, J. W. L. Jr, and M. Belaval, "Continuous resistivity profiling to delineate submarine groundwater discharge-examples and limitations," *The Leading Edge*, vol. 25, no. 6, pp. 724–728, 2006.

[3] A. Ruffell and J. McKinley, "Forensic geoscience: applications of geology, geomorphology and geophysics to criminal investigations," *Earth-Science Reviews*, vol. 69, no. 3-4, pp. 235–247, 2005.

[4] A. Ziolkowski and D. Wright, "The potential of the controlled source electromagnetic method: A powerful tool for hydrocarbon exploration, appraisal, and reservoir characterization," *IEEE Signal Processing Magazine*, vol. 29, no. 4, pp. 36–52, 2012.

[5] T. Günther, C. Rücker, and K. Spitzer, "3-d modeling and inversion of dc resistivity data incorporating topography - part ii: Inversion," *Geophysical Journal International*, vol. 166, pp. 506–517, 2006.

[6] S. A. Bakr and T. Mannseth, "An approximate hybrid method for electromagnetic scattering from an underground target," *IEEE Transactions on Geoscience and Remote Sensing*, vol. 51, no. 1, 2013.

[7] D. S. Holder, *Electrical Impedance Tomography: Methods, History and Applications*. Institute of Physics, 2004.

[8] J. Kaipio and E. Somersalo, *Statistical and Computational Inverse Problems*, ser. Applied Mathematical Sciences. Springer, 2005.

[9] H. Ammari and H. Kang, *Polarization and Moment Tensors with applications to inverse problems and effective medium theory*. Springer, 2007.

[10] H. Ammari, J. Garnier, W. Jing, H. Kang, M. Lim, K. Sølna, and H. Wang, *Mathematical and Statistical Methods for Multistatic Imaging*. Springer, 2013.

[11] H. Ammari and H. Kang, "Generalized polarization tensors, inverse conductivity problems, and dilute composite materials: a review." *Contemporary Mathematics*, vol. 408, pp. 1–67, 2006.

[12] O. Kwon, J. K. Seo, and J.-R. Yoon, "A real time algorithm for the location search of discontinuous conductivities with one measurement," *Communications on Pure and Applied Mathematics*, vol. 55, no. 1, pp. 1–29, 2002.

[13] M. Hanke, "On real-time algorithms for the location search of discontinuous conductivities with one measurement," *Inverse Problems*, vol. 24, no. 4, 2004.

[14] G. Dassios and A. S. Fokas, "Electro-magneto-encephalography for a three-shell model: dipoles and beyond for the spherical geometry," *Inverse Problems*, vol. 25, no. 3, p. 035001, 2009.

[15] H. Ammari and J. K. S. Seo, "An accurate formula for the reconstruction of conductivity inhomogeneities," *Advances in Applied Mathematics*, vol. 30, no. 4, pp. 679–705, 2003.

[16] H. Ammari, O. Kwon, J. K. Seo, and E. J. Woo, "T-scan electrical impedance imaging system for anomaly detection," *SIAM Journal on Applied Mathematics*, vol. 65, no. 1, pp. 252–266, 2004.

[17] A. Kirsch, *An Introduction to the Mathematical Theory of Inverse Problems*. Springer, 2011, ch. 5.

[18] M. Hanke and B. Schappel, "The factorization method for electrical impedance tomography in the half-space," *SIAM Journal on Applied Mathematics*, vol. 68, no. 4, pp. 907–924, 2008.

[19] H. Ammari, R. Griesmaier, and M. Hanke, "Identification of small inhomogeneities: Asymptotic factorization," *Mathematics of Computation*, vol. 76, no. 259, pp. 1425–1448, 2007.

[20] F. Delbary and R. Kress, "Electrical impedance tomography with point electrodes," *Journal of Integral Equations and Applications*, vol. 22, no. 2, pp. 193–216, 2010.

[21] H. Ammari, T. Boulier, J. Garnier, W. Jing, H. Kang, and H. Wang, "Target identification using dictionary matching of generalized polarization tensors," *Foundations of Computational Mathematics*, vol. 14, no. 1, pp. 27–62, 2014.

[22] H. Ammari, J. Garnier, H. Kang, M. Lim, and S. Yu, "Generalized polarization tensors for shape description," *Numerical Mathematics*, vol. 126, no. 2, pp. 199–224, 2014.

[23] N. Polydorides, E. Storteig, and W. Lionheart, "Forward and inverse problems in towed cable hydrodynamics," *Ocean Engineering*, vol. 35, no. 14, pp. 1429–1438, 2008.

[24] H. Ammari, H. Kang, E. Kim, and M. Lim, "Reconstruction of closely spaced small inclusions," *SIAM Journal on Numerical Analysis*, vol. 42, no. 6, pp. 2408–2428, 2005.

[25] D. Colton and R. Kress, *Inverse acoustic and electromagnetic scattering theory*, 3rd ed., ser. Applied Mathematical Sciences. Springer, New York, 2013, vol. 93. [Online]. Available: http://dx.doi.org/10.1007/978-1-4614-4942-3

[26] J. W. Demmel, *Applied Numerical Linear Algebra*. SIAM, 1997.

[27] L. Reichel and Q. Ye, "Simple square smoothing regularization operators," *Electronic Transactions on Numerical Analysis*, vol. 33, pp. 63–83, 2009.

[28] M. Wang, Y. Ma, N. Holliday, Y. Dai, R. Williams, and G. Lucas, "A high-performance eit system," *IEEE Sensors Journal*, vol. 5, no. 2, pp. 289–299, 2005.

[29] F. Day-Lewis, E. A. White, C. D. Johnson, and J. W. Lane-Jr, "Continuous resistivity profiling to delineate submarine groundwater discharge-examples and limitations," *The Leading Edge*, vol. 25, no. 6, pp. 724–728, 2006.

[30] J. A. Breier, C. F. Breier, and H. N. Edmonds, "Detecting submarine groundwater discharge with synoptic surveys of sediment resistivity, radium and salinity," *Geophysical Research Letters*, vol. 32, p. L23612, 2005.